Orientation dependent cyclic stability of the elastocaloric effect in textured Ni-Mn-Ga alloys

Longsha Wei, ⬥ **Xuexi Zhang,** ⬥ **Jian Liu, et al.**

View Online   Export Citation   CrossMark

ARTICLES YOU MAY BE INTERESTED IN

AIP Advances

Mathematical Physics Collection

READ NOW

Orientation dependent cyclic stability of the elastocaloric effect in textured Ni-Mn-Ga alloys

Longsha Wei,[1] Xuexi Zhang,[1,a] Jian Liu,[2] and Lin Geng[1]

[1]*School of Materials Science and Engineering, Harbin Institute of Technology, Harbin 150001, PR China*
[2]*Key Laboratory of Magnetic Materials and Devices, Ningbo Institute of Material Technology and Engineering, CAS, Ningbo 315201, PR China*

High-performance elastocaloric materials require a large reversible elastocaloric effect and long life cyclic stability. Here, we fabricated textured polycrystalline $Ni_{50.4}Mn_{27.3}Ga_{22.3}$ alloys by cost-effective casting method to create a <001> texture. A strong correlation between the cyclic stability and the crystal orientation was demonstrated. A large reversible adiabatic temperature change ΔT ~6 K was obtained when the external stress was applied parallel to <001> direction. However, the ΔT decreased rapidly after 50 cycles, showing an unstable elastocaloric effect (eCE). On the other hand, when the external stress was applied perpendicular to <001>, the adiabatic ΔT was smaller ~4 K, but was stable over 100 cycles. This significantly enhanced eCE stability was related to the high yield strength, low transformation strain and much higher crack initiation-propagation resistances perpendicular to <001> direction. This study provides a feasible strategy for optimizing the eCE property by creation of the texture structure in polycrystalline Ni-Mn-Ga and Ni-Mn-X (X= In, Sn, Sb) alloys. © *2018 Author(s). All article content, except where otherwise noted, is licensed under a Creative Commons Attribution (CC BY) license (http://creativecommons.org/licenses/by/4.0/).* https://doi.org/10.1063/1.5028212

Recently, the solid-state refrigeration based on the elastocaloric effect (eCE) has been emerging as a promising candidate technique for the conventional vapor-compression refrigeration.[1] Giant adiabatic temperature changes (ΔT) have been realized in shape memory alloys, such as 25 K in $Ni_{50}Ti_{50}$[2] and 13 K in $Cu_{71.5}Al_{17.5}Mn_{11}$.[3] Ni-Mn-based ferromagnetic shape memory alloys (FMSMAs), including Ni-Mn-Ga and Ni-Mn-X (X=In, Sn, Sb), exhibited multifunctional properties including magnetic-field-induced strain (MFIS),[4] magnetic shape memory effect,[5] magnetoresistance,[6] magnetocaloric effect (MCE)[7] and eCE.[8] It was reported that stress-induced ΔT in Ni-Mn-Sn and Ni-Mn-In-Co alloys reached 3-9.5 K,[9,10] which were comparable to that induced by a high magnetic field.[11]

The application of elastocaloric refrigeration requires a large reversible ΔT and good cyclic stability during multiple stress cycles. However, the metamagnetic Ni-Mn-X (X = In, Sn, Sb) alloys usually exhibit a distinct irreversibility during loading-unloading cycles[9] because of the elastic incompatibility of the martensite/austenite interface and the formation of dislocations or micro-cracks.[12,13] Moreover, the reversibility is important for high cyclic stability and thus a long functional fatigue life.[14] Improvement of the martensite transformation (MT) reversibility may be realized by tuning the geometric compatibility between A/M interface.[15,16] The thermodynamic process during MT also affects the reversibility.[17] For example, in Ni-Ti alloys, the transformation hysteresis of B2-R is smaller than that of B2-B19', implying a better elastocaloric reversibility during B2-R cycling.[18] In Ni-Mn-Ga alloys, the austenite↔5M martensite exhibited the most promising eCE due to the low superelastic critical stress and small transition strain,[19] which benefit for a long fatigue life. In single crystalline Ni-Mn-Ga alloys, only 5M martensite could be formed under

---

[a]Corresponding author. Tel: 86-451-86415894, Fax: 86-451-86413921, Email: xxzhang@hit.edu.cn

compressive stress along <001> direction because the stress-induced intermartensite transformation was prevented.[20,21]

Single crystalline FMSMAs such as Ni-Fe-Ga,[14] Co-Ni-Ga[22] showed good reversibility and fatigue life during stress-cycling. However, their polycrystalline alloys are brittle. It is effective to enhance the ductility by micro-alloying[23] or by reducing intergranular constraints through texture.[24,25] For example, a stable $\Delta T = 4$ K over 200 cycles was achieved in a <001> textured $Ni_{49.5}Mn_{28}Ga_{22.5}$ alloy.[25] However, further work is needed to build a relationship between crystal orientation and cyclic stability of eCE. Here, this relationship was demonstrated in a textured $Ni_{50.4}Mn_{27.3}Ga_{22.3}$ alloy: Smaller ΔT but enhanced cyclic stability when loading perpendicular to <001> direction than parallel to it. This provides a feasible strategy to optimize the microstructural and loading direction for stable eCE.

Polycrystalline $Ni_{50.4}Mn_{27.3}Ga_{22.3}$ (at.%) rectangular plate was prepared by melting pure Ni, Mn and Ga metals (purity >99.95%) under argon atmosphere in a vacuum induction furnace and casting into a graphite mold with size 200×100×25 mm. The composition of the plate was determined by energy dispersion spectrum (EDS). Compressive samples for eCE tests with size of 4×4×8 mm^3 were prepared by electron discharge machining (EDM). The samples were sealed into a quartz tube, vacuumed and then subjected to a stepwise annealing heat treatment (1273 K 10 h, 998 K 2 h, 973 K 10 h and 773 K 20 h) for compositional homogenization and chemical ordering. After annealing, the martensite structure was examined by X-ray diffraction (XRD) with Cu-Kα radiation. The grains along the solidification direction (SD) of the plate was analyzed using a scanning electronic microscope (SEM) equipped with electron back-scattered diffraction (EBSD) at a temperature of 370 K. The martensite transformation was monitored in a TA Discovery-2500 differential scanning calorimeter (DSC). The heat capacity was determined by T4P Tzero® heat flow technology. The superelastic cycling tests were performed in an Instron 5500R universal testing machine and the adiabatic temperature change ΔT_{expt} was recorded using a T-type thermocouple welded on the sample surface. The temperature data were recorded by an OM-DAQ-USB-2401 data acquisition module with a working frequency 1 Hz. The measurement accuracy of the thermocouple is ±1.1 K.

The MT temperatures of the annealed $Ni_{50.4}Mn_{27.3}Ga_{22.3}$ alloy were determined by DSC (Fig. S1a of the supplementary material). The corresponding first-order MT temperatures (M_s, M_f, A_s, A_f) and second-order Curie point (T_c) are listed in Table I. The thermal hysteresis A_f - M_s was determined to be 9 K. Such low thermal hysteresis may favor the reversible superplasticity. The enthalpy change (ΔH) and entropy change ($\Delta S = \Delta H/T_0$, where $T_0 = (M_s + A_f)/2$[26]) are also summarized in Table I. Given a complete MT during superelastic cycling, the adiabatic temperature change limit may be theoretically calculated by $|\Delta T_t| = |(T \times \Delta S)/C_p| = 8.8$ K, where the heat capacity C_p was determined to be 610 J/kg K (Fig. S1b of the supplementary material).

XRD patterns confirmed the existence of the 5M martensite in the $Ni_{50.4}Mn_{27.3}Ga_{22.3}$ alloy at room temperature (Fig. S2 of the supplementary material), which is beneficial for the low superelastic critical stress and small transition strain.[20] Fig. 1a shows coarse columnar grains in the austenite state at a temperature of 370 K. The axis of the columnar grains was parallel to the <001> crystal direction, as shown by the pole figure in Fig. 1b. The transformation strains of the austenite↔5M was calculated according to the Lattice Deformation Theory (LDT),[27] using the lattice parameters: austenite $a = 5.823$ Å, 5M martensite $a = 5.919$ Å and $c = 5.584$ Å obtained from Fig. S2 of the supplementary material. The result illustrated in Fig. 1c shows that the transformation strain along the <001> direction was the largest (4.1%), but smallest along <111> direction, implying a large crystal orientation dependent transformation strain in textured Ni-Mn-Ga alloys.

TABLE I. Martensite transformation temperatures (M_s, M_f, A_s, A_f), Curie point (T_C), the enthalpy change (ΔH) and thermal-induced transition entropy change (ΔS) during cooling (ΔH_c, ΔS_c) and heating (ΔH_h, ΔS_h) process of the $Ni_{50.4}Mn_{27.3}Ga_{22.3}$ alloy determined by DSC.

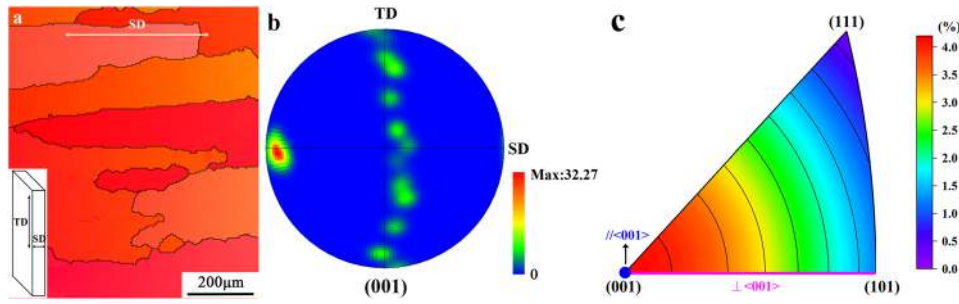| Transformation temperature, K					Enthalpy change, J/g		Entropy change, J/kgK	
M_f	M_s	A_s	A_f	T_c	$|\Delta H_c|$	$|\Delta H_h|$	$|\Delta S_c|$	$|\Delta S_h|$
308	314	318	323	369	5.22	5.15	16.4	16.2

FIG. 1. a) Inverse pole figure (IPF) map and b) pole figure showing columnar grains that grow along the solidification direction (SD) in the $Ni_{50.4}Mn_{27.3}Ga_{22.3}$ alloy obtained at a temperature of 370 K. The inset of a) schematically shows the rectangular alloy plate prepared by casting. c) illustrates the orientation dependent transformation strain map related to austenite↔5M transition. The colors represent the transformation strains.

Fig. 2a and 2b displays the superelastic curves when the compressive direction (CD) is parallel and perpendicular to <001>, respectively. At a temperature of 317 K (slightly lower than As, 318 K), a superelastic stress plateau appeared during loading, but with a large residual strain upon unloading. The residual strain completely disappeared at a higher temperature of 322 K (close to A_f = 323 K). At temperatures >A_f, the alloy shows fully reversible superelastic behavior with a maximum recoverable strain of 2.2% and 1.5% parallel and perpendicular to <001>, respectively. The critical stress σ_{Ms} was smaller while the maximum recoverable strain was larger along <001> than those perpendicular to <001>. The theoretical strain parallel to <001> is 4.1%, as shown by blue circle in Fig. 1c, and the strain perpendicular to <001> is 2.8%, which is the average strain of direction perpendicular to <001>, i.e. the pink line in Fig. 1c. As a result, the critical stress that triggers the austenite to martensite transition parallel to <001> was lower than that perpendicular to <001> according to the Clausius-Clapeyron equation $d\sigma/dT = (\Delta S \times \rho)/\Delta\varepsilon$.[28] The experimental reversible strains in both directions were about half of the theoretical strains due to the grain boundary restriction on the favorable single variant formation.[29] The stress hysteresis, defined as the stress difference between the loading/unloading plateaus (arrows in Fig. 2a), were 27 and 34 MPa at 327 K parallel and perpendicular to <001>, respectively, both decreasing with temperature. The low stress hysteresis obtained by taking advantage of the austenite↔5M transformation contributes to the enhanced reversibility of eCE.[19]

From Fig. 2, the MT critical stresses (σ_{As} and σ_{Ms}) were shown in Fig. S3 of the supplementary material. The slope $d\sigma/dT$ in both directions was 3 MPa/K for the austenite to martensite forward transformation, and 4-4.4 MPa/K for the backward transformation. The obtained critical stress is
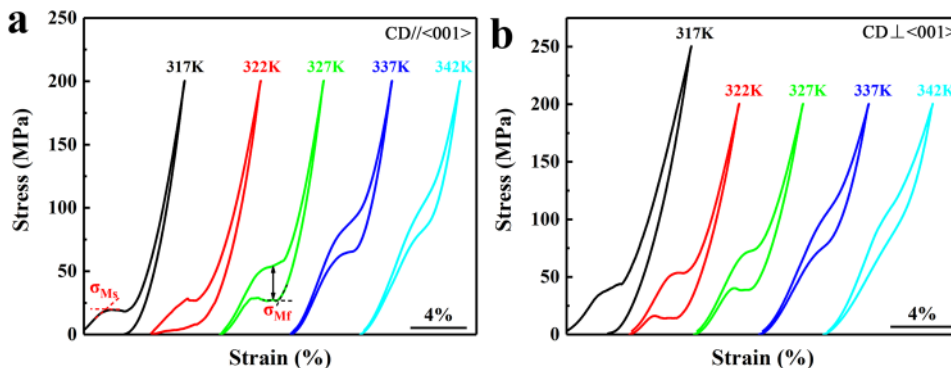

FIG. 2. Compressive superelastic curves of the $Ni_{50.4}Mn_{27.3}Ga_{22.3}$ alloy at different temperatures under a strain rate of 4×10^{-4} s^{-1}. The compressive direction is a) parallel and b) perpendicular to <001> direction. σ_{Ms} and σ_{Mf} marked in a) refer to the martensite and austenite formation critical stresses, respectively. The arrows marked in a) defines the stress hysteresis of the superelastic cycle.

similar to that in Ni-Mn-Ga single crystals,[20] implying that martensite/austenite interface movement resistance in this $Ni_{50.4}Mn_{27.3}Ga_{22.3}$ alloy was as low as that in single crystals attributed to the coarse columnar grains and <001> texture.

In order to investigate the reversibility of the adiabatic temperature change (ΔT), loading/unloading cycling compressive test was conducted. The holding time between loading and unloading processes was 30 s, allowing for the full temperature equilibration in the specimen. The ΔT – time (t) curves are displayed in Fig. 3. It is noted from Fig. 3a that ΔT_{expt} reached 6.1 K upon loading and 6.5 K upon unloading when the compressive direction was parallel to <001>, which are smaller than the theoretical ΔT_t = 8.8 K and are comparable to Ni-Fe-Ga single crystals ΔT = 7.5 K.[30] The smaller ΔT_{expt} was thought to be related to the incomplete superelastic transition and inhomogeneous temperature distribution in the sample.[22] ΔT perpendicular to <001> direction, i.e. 3.3 K upon loading and 4.1 K upon unloading (Fig. 3b), are comparable to those in polycrystalline $Ni_{48}Mn_{35}In_{17}$[31] and $Ni_{45}Mn_{36.4}In_{13.6}Co_{5.1}$[32] alloys.

Of note is that the obtained ΔT perpendicular to the <001> direction is lower than that along <001> direction. This is probably related to the high superelastic critical stresses that only incomplete superelastic behavior occured perpendicular to <001>, as shown in the inset in Fig. 3b. A larger ΔT could be obtained under increasing applied stress or decreasing temperature, as verified in Fig 3c. The fact that $|\Delta T_{expt-loading}|<|\Delta T_{expt-unloading}|$ is in agreement with the Clausius-Clapeyron relationship in which the slope of the unloading process (4 - 4.4 MPa/K) is higher than that of loading process (3 MPa/K), as shown in Fig. S3a of the supplementary material. However, this is not
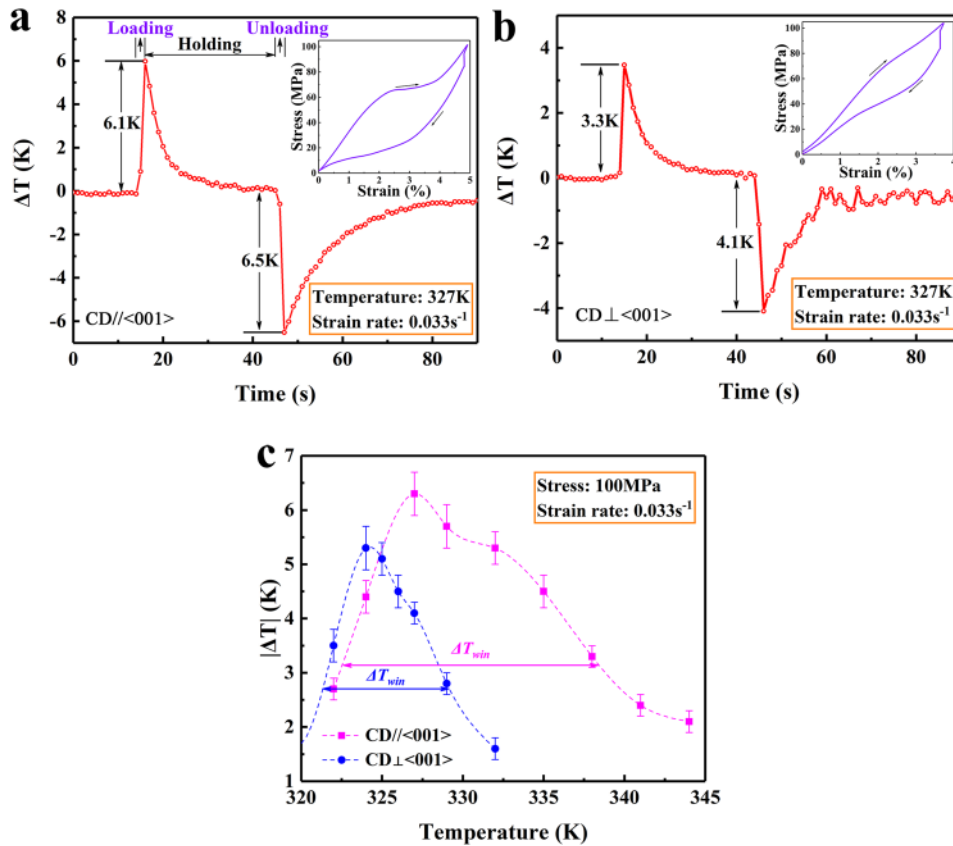

FIG. 3. The adiabatic temperature changes ΔT of the $Ni_{50.4}Mn_{27.3}Ga_{22.3}$ alloy at a temperature of 327 K and strain rate of 0.033 s^{-1}. The compressive direction is a) parallel and b) perpendicular to <001> direction, respectively. The insets of a) and b) represent the corresponding superelastic curves during ΔT tests. c) shows the temperature dependent ΔT for compressive direction CD//<001> and CD⊥<001>, respectively. The ΔT_{win} represent the working temperature window denoted as the full width at half maximum of the ΔT peak.

agree with NiTi wires[33] and Ni-Mn-In-Co alloys,[9] in which $|\Delta T_{expt\text{-}loading}| > |\Delta T_{expt\text{-}unloading}|$ due to their intrinsic heat dissipation behavior.[33] A larger $|\Delta T_{expt\text{-}unloading}|$ may be attributed to the additional MT during stress holding process, which has also been reported in $Ni_{45}Mn_{36}In_{14}Co_5$[34] and $Ni_{54}Fe_{19}Ga_{27}$ alloy[35] alloys. This phenomenon implies that the cooling effect from additional transformation upon unloading exceeds the heating effect from frictional heating in the $Ni_{50.4}Mn_{27.3}Ga_{22.3}$ alloy. The irreversible temperature change related to the intrinsic heat dissipation,[33] calculated based on the hysteresis area in the stress-strain curve at 327 K in Fig. 2, was determined to be 0.2 K in both directions and is much smaller than those of Ni-Ti wires[33] and Ni-Mn-In-Co bulk alloys.[9]

Fig. 3c shows ΔT during a fast unloading process under a maximum stress of 100 MPa. The largest $|\Delta T|$ parallel and perpendicular to <001> are 6.3 K and 5.3 K, corresponding to the test temperatures of 327 K and 324 K, respectively. For caloric materials, the working temperature window ΔT_{win}, defined as the full width at half maximum of ΔS or ΔT,[36] is also an important factor to evaluate the cooling capacity. Here under a low stress of 100 MPa, a high $\Delta T_{win} = 16$ K was obtained along <001>, which is smaller than that of the $Ni_{50}Fe_{19}Ga_{27}Co_4$ single crystal 28 K[37] but is comparable to those of $Ni_{43}Mn_{46}Sn_{11}$[38] (~8 K), $Ni_{44.5}Mn_{36.4}In_{14}Co_{5.1}$[39] (~12 K) and $Ni_{43}Mn_{43}Co_3Sn_{11}$[40] (~12 K) compounds. It can also be seen from Fig. 3c that ΔT_{win} perpendicular to <001> direction (8 K) was smaller than that parallel to <001> (16 K) because the higher critical stresses perpendicular to <001>, as displayed in Fig. 2. As experimentally verified in $Cu_{68}Zn_{16}Al_{16}$ and $Ni_{50}Fe_{19}Ga_{27}Co_4$ alloys,[37,41] ΔT_{win} increased with external applied stress, showing that even broader ΔT_{win} can be obtained. Supposing a full MT induced by stress, ΔT would be equivalent in directions parallel and perpendicular to <001> since the transition entropy change is independent on crystal orientation.[42]

For a caloric material, the figures-of-merit, such as Coefficient of Refrigerant Performance (CRP),[43] Relative Cooling Power (RCP)[44] and Temperature averaged Entropy Change (TEC),[45] is useful to evaluate the refrigeration capacity and refrigeration efficiency calculated by isothermal entropy change. For the direct method, the specific caloric effects, defined as $|\Delta T/\Delta\sigma|$ and $|\Delta T/\Delta\varepsilon|$, reflect the caloric efficiency and energy conversion ratio. A low $\Delta\sigma$ implies less energy and feasibility for eCE, while a small $\Delta\varepsilon$ contributes to a longer fatigue life and miniaturization of the refrigeration device. The adiabatic temperature and specific caloric effects of the present alloy, some conventional and ferromagnetic shape memory alloys are summarized in Table II. Most shape memory alloys display only high $|\Delta T/\Delta\sigma|$ or $|\Delta T/\Delta\varepsilon|$, while the present $Ni_{50.4}Mn_{27.3}Ga_{22.3}$ alloy shows both high $|\Delta T/\Delta\sigma|$ and high $|\Delta T/\Delta\varepsilon|$. This implies that the present $Ni_{50.4}Mn_{27.3}Ga_{22.3}$ alloy shows a high efficiency to convert mechanical work to heat.

The cyclic stability of eCE was performed by the superplastic cycling under a strain rate of 0.033 s^{-1} and temperature of 327 K, as shown in Fig. 4. The σ_{Ms} decreases with increasing cycle number in the two orientations. This is related to the stress fields of the residual martensite trapped by dislocations, which oriented favorably to accommodate the applied stress.[24] Before 50th cycles, the transformation strains in both directions kept intact and fully recovered during unloading (Fig. 4a). It is also interesting to found that the maximum strain increased rapidly between 50-63th cycles along <001>, while the strain changed little up to 100 cycles perpendicular to <001> (Fig. 4b). This phenomenon is consistent to the damage behavior of the samples, as shown in the insets in Fig. 4a

TABLE II. A comparison of adiabatic temperature change (ΔT) and specific adiabatic temperature change ($|\Delta T/\Delta\sigma|$ and $|\Delta T/\Delta\varepsilon|$) for the present $Ni_{50.4}Mn_{27.3}Ga_{22.3}$ alloy, some conventional and ferromagnetic shape memory alloys.

| Materials	Sample status	ΔT, K	$|\Delta T/\Delta\sigma|$, K/GPa	$|\Delta T/\Delta\varepsilon|$, K/1%	Reference
$Ni_{50.4}Mn_{27.3}Ga_{22.3}$ (//<001>)	Texture polycrystal	6.5	65	3	Present
$Ni_{50.4}Mn_{27.3}Ga_{22.3}$ (⊥<001>)	Texture polycrystal	4.1	53	3.1	Present
$Ni_{54}Fe_{19}Ga_{27}$	Single crystal	7.5	83	2	30
$Ni_{45}Mn_{36.5}In_{13.5}Co_5$	Texture polycrystal	8.6	34.4	2.2	9
$Co_{50}Ni_{30}Ga_{20}$	Single crystal	6	40	1.7	22
$Ni_{48.9}Ti_{51.1}$	Wire	25	31.25	5	33
$Cu_{71.5}Al_{17.5}Mn_{11}$	Texture polycrystal	13	72	1.5	3
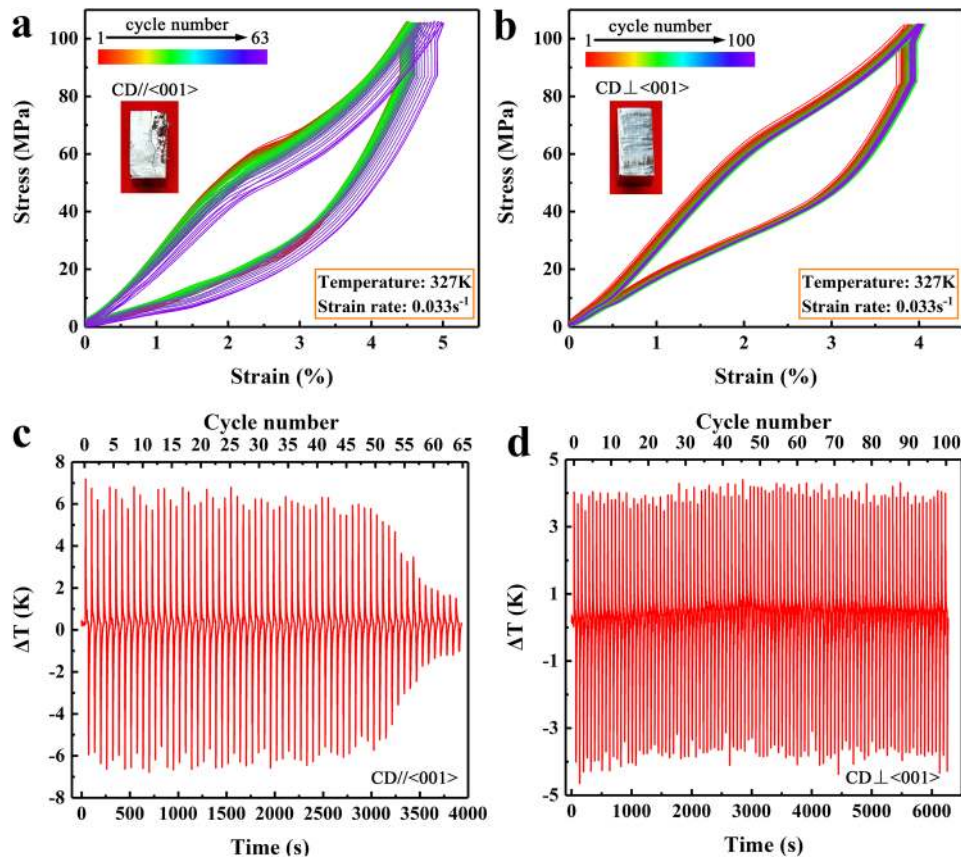
FIG. 4. Compressive superelastic cycling curves (a, b) and corresponding adiabatic temperature change $\varDelta T$ (c, d) at a temperature of 327 K and strain rate of 0.033 s^{-1} in the Ni$_{50.4}$Mn$_{27.3}$Ga$_{22.3}$ alloy. The compressive direction is a) parallel and b) perpendicular to <001> direction, respectively. The inset macro-images of a) and b) show the morphology of the samples after 63 and 100 cycles. c) and d) are time dependent $\varDelta T$ in the directions parallel and perpendicular to <001> direction, respectively.

and 4b, in which serious damage occurred in the samples stressed along <001> due to the plastic deformation. Overall, the alloy exhibited a high $\varDelta T$ but unstable cycling stability along <001>, and an enhanced stability but smaller $\varDelta T$ perpendicular to <001>. Given that elastocaloric cooling requires many cycles with little fatigue behavior, the application of eCE perpendicular to <001> direction is more favorable.

The $\varDelta T$ profiles parallel and perpendicular to <001> directions are illustrated in Fig. 4c–d. Fig. 4c showed that, along <100> direction, a stable $\varDelta T$ ~6 K existed in 50 cycles but rapidly decreased with increasing cycles. The $\varDelta T$ perpendicular to <001> direction, however, kept stable in 100 cycles, with $\varDelta T$ ~4 K during loading/unloading processes (Fig. 4d), indicating a good stability and reversibility of the eCE behavior. The good cyclic stability is comparable to the dual-phase containing Ni$_{54}$Fe$_{19}$Ga$_{27}$[35] and (Ni$_{51.5}$Mn$_{33}$In$_{15.5}$)$_{99.7}$B$_{0.3}$[23] alloys. Here the improvement in the cyclic stability was achieved by introducing a <001> texture rather than a second phase. A high cyclic stability over 200 cycles with stable $\varDelta T$ = 4 K along <001> direction was also found in a Ni$_{49.5}$Mn$_{28}$Ga$_{22.5}$ alloy prepared by a directional solidification method.[25] Considering the eCE properties along <001>, the obtained stable $\varDelta T$ = 6 K in the present alloy is higher than that reported in Ref. 25, but the stable cycles in this work (50 cycles) are smaller than that in Ref. 25 (200 cycles), probably due to the high defect density and transformation strain, and the existence of the triple grain junctions (Fig. 1a). The present work further demonstrated that the cyclic stability showed a strong orientation dependence, i.e. enhanced fatigue behavior perpendicular to <001> because of the small transformation strain, high dislocation slip resistance[46] and low energy dissipation.[47] The higher crack initiation/propagation resistances

perpendicular to <001> direction[24] under a compressive stress state also contributed to the high fatigue behavior.

In summary, we demonstrated the strong crystal orientation dependent cyclic stability of the eCE in a <001> textured $Ni_{50.4}Mn_{27.3}Ga_{22.3}$ alloy. A large ΔT up to ~6 K may be obtained along <001> direction, however decreased rapidly after 50 cycles. On the other hand, a stable ΔT ~4 K over 100 cycles was achieved when stressing perpendicular to <001>. The enhanced cyclic stability was attributed to the high yield strength, low transformation strain, low energy dissipation and high crack initiation/propagation resistances perpendicular to <001> direction. This work provides a feasible strategy for optimizing the eCE property by creation of the texture structure in polycrystalline Ni-Mn-Ga and Ni-Mn-X (X= In, Sn, Sb) alloys.

See supplementary material for the martensite transformation, 5M martensite phase and temperature dependent superelastic stresses of the studied $Ni_{50.4}Mn_{27.3}Ga_{22.3}$ alloy.

[1] W. Goetzler, R. Zogg, J. Young, and C. Johnson, US Department of Energy (2014).
[2] J. Cui, Y. M. Wu, J. Muehlbauer, Y. H. Hwang, R. Radermacher, S. Fackler, M. Wuttig, and I. Takeuchi, Appl. Phys. Lett. **101**, 0739047 (2012).
[3] S. Xu, H. Y. Huang, J. X. Xie, S. Takekawa, X. Xu, T. Omori, and R. Kainuma, APL Mater. **4**(10), 106106 (2016).
[4] K. Ullakko, J. K. Huang, C. Kantner, R. C. OHandley, and V. V. Kokorin, Appl. Phys. Lett. **69**(13), 1966 (1996).
[5] O. Heczko, J Magn Magn Mater. **290**, 787 (2005).
[6] C. Biswas, R. Rawat, and S. R. Barman, Appl. Phys. Lett. **86**, 20250820 (2005).
[7] T. Krenke, E. Duman, M. Acet, E. F. Wassermann, X. Moya, L. Manosa, and A. Planes, Nat Mater. **4**(6), 450 (2005).
[8] B. F. Lu, F. Xiao, A. Yan, and J. Liu, Appl. Phys. Lett. **105**, 161905 (2014).
[9] D. W. Zhao, J. Liu, Y. Feng, W. Sun, and A. Yan, Appl. Phys. Lett. **110**, 021906 (2017).
[10] W. Sun, J. Liu, B. F. Lu, Y. Li, and A. Yan, Scr. Mater. **114**, 1 (2016).
[11] J. Liu, T. Gottschall, K. P. Skokov, J. D. Moore, and O. Gutfleisch, Nat Mater. **11**(7), 620 (2012).
[12] J. Cui, Y. S. Chu, O. O. Famodu, Y. Furuya, J. Hattrick-Simpers, R. D. James, A. Ludwig, S. Thienhaus, M. Wuttig, Z. Y. Zhang, and I. Takeuchi, Nat Mater. **5**(4), 286 (2006).
[13] Z. Y. Zhang, R. D. James, and S. Muller, Acta Mater. **57**(15), 4332 (2009).
[14] Y. Wu, E. Ertekin, and H. Sehitoglu, Acta Mater. **135**, 158 (2017).
[15] Y. Song, X. Chen, V. Dabade, T. W. Shield, and R. D. James, Nature **502**(7469), 85 (2013).
[16] E. Stern-Taulats, A. Planes, P. Lloveras, M. Barrio, S. Tamarit, S. Pramanick, S. Majumdar, S. Yuce, B. Emre, C. Frontera, and L. Manosa, Acta Mater. **96**, 324 (2015).
[17] D. Z. Xue, P. V. Balachandran, J. Hogden, J. Theiler, D. Q. Xue, and T. Lookman, Nat Commun. **7**, 11241 (2016).
[18] D. Soto-Parra, E. Vives, L. Manosa, J. A. Matutes-Aquino, H. Flores-Zuniga, and A. Planes, Appl. Phys. Lett. **108**, 071902 (2016).
[19] V. A. Chernenko, E. Villa, D. Salazar, and J. M. Barandiaran, Appl. Phys. Lett. **108**(7) (2016).
[20] V. A. Chernenko, J. Pons, E. Cesari, and K. Ishikawa, Acta Mater. **53**(19), 5071 (2005).
[21] V. V. Martynov and V. V. Kokorin, J Phys III **2**(5), 739 (1992).
[22] A. Shen, D. W. Zhao, W. Sun, J. Liu, and C. J. Li, Scr. Mater. **127**, 1 (2017).
[23] Z. Yang, D. Y. Cong, X. M. Sun, Z. H. Nie, and Y. D. Wang, Acta Mater. **127**, 33 (2017).
[24] R. F. Hamilton, H. Sehitoglu, C. Efstathiou, H. J. Maier, and Y. Chumlyakov, Acta Mater. **54**(3), 587 (2006).
[25] Y. Hu, Z. B. Li, B. Yang, S. X. Qian, W. M. Gan, Y. Y. Gong, Y. Li, D. W. Zhao, J. Liu, X. Zhao, L. Zuo, D. H. Wang, and Y. W. Du, APL Mater. **5**(4) (2017).
[26] H. C. Tong and C. M. Wayman, Acta Metallurgica **22**(7), 887 (1974).
[27] S. Miyazaki and C. M. Wayman, Acta Metallurgica **36**(1), 181 (1988).
[28] X. Moya, S. Kar-Narayan, and N. D. Mathur, Nat Mater. **13**(5), 439 (2014).
[29] M. Kimiecik, J. W. Jones, and S. Daly, Acta Mater. **94**, 214 (2015).
[30] Y. Li, D. W. Zhao, and J. Liu, Sci Rep-Uk **6**, 25500 (2016).
[31] Y. J. Huang, Q. D. Hu, N. M. Bruno, J. H. Chen, I. Karaman, J. H. Ross, and J. G. Li, Scr. Mater. **105**, 42 (2015).
[32] B. F. Lu, P. N. Zhang, Y. Xu, W. Sun, and J. Liu, Mater. Lett. **148**, 110 (2015).
[33] J. Tusek, K. Engelbrecht, L. P. Mikkelsen, and N. Pryds, J. Appl. Phys. **117**(12) (2015).
[34] B. F. Lu and J. Liu, Sci Rep-Uk **7** (2017).
[35] Y. Xu, B. F. Lu, W. Sun, A. Yan, and J. Liu, Appl. Phys. Lett. **106**, 201903 (2015).
[36] K. A. Gschneidner, V. K. Pecharsky, and A. O. Tsokol, Rep Prog Phys. **68**(6), 1479 (2005).
[37] F. Xiao, M. J. Jin, J. Liu, and X. J. Jin, Acta Mater. **96**, 292 (2015).
[38] Y. Zhang, Q. Zheng, W. X. Xia, J. Zhang, J. Du, and A. Yan, Scr. Mater. **104**, 41 (2015).
[39] X. Zhang, M. Qian, S. Miao, R. Su, Y. Liu, L. Geng, and J. Sun, J. Alloy. Compd. **656**, 154 (2016).
[40] B. Gao, F. X. Hu, J. Shen, J. Wang, J. R. Sun, and B. G. Shen, J Magn Magn Mater. **321**(17), 2571 (2009).
[41] L. Manosa, S. Jarque-Farnos, E. Vives, and A. Planes, Appl. Phys. Lett. **103**, 211904 (2013).
[42] N. M. Bruno, I. Karaman, and Y. I. Chumlyakov, Phys Status Solidi B **255**(2) (2018).

[43] M. E. Wood and W. H. Potter, Cryogenics **25**(12), 667 (1985).
[44] K. A. Gschneidner and V. K. Pecharsky, Annu Rev Mater Sci. **30**, 387 (2000).
[45] L. D. Griffith, Y. Mudryk, J. Slaughter, and V. K. Pecharsky, J. Appl. Phys. **123**(3) (2018).
[46] K. Gall and H. Maier, Acta Mater. **50**(18), 4643 (2002).
[47] E. E. Timofeeva, E. Y. Panchenko, N. G. Vetoshkina, Y. I. Chumlyakov, A. I. Tagiltsev, A. S. Eftifeeva, and H. Maier, Russ. Phys. J. **59**(8), 1251 (2016).